JOURNAL OF SCIENCE
SAKARYA UNIVERSITY

Sakarya University Journal of Science

ISSN 1301-4048 | e-ISSN 2147-835X | Period Bimonthly | Founded: 1997 | Publisher Sakarya University | http://www.saujs.sakarya.edu.tr/

Title: Analysis of The Performance of The NOSM For High Contrast Targets

Authors: Mehmet Nuri Akıncı
Recieved: 2018-10-16 00:00:00
Revised: 2018-10-28 12:00:00
Accepted: 2018-11-10 00:00:00
Article Type: Research Article
Volume: 23
Issue: 2
Month: April
Year: 2019
Pages: 224-232

How to cite
Mehmet Nuri Akıncı; (2019), Analysis of The Performance of The NOSM For High Contrast Targets. Sakarya University Journal of Science, 23(2), 224-232, DOI: 10.16984/saufenbilder.471026
Access link
http://www.saujs.sakarya.edu.tr/issue/39539/471026

Sakarya University Journal of Science 23(2), 224-232, 2019

Analysis of the Performance of the Near Field Orthogonality Sampling Method for Microwave Imaging of High Contrast Targets

Mehmet Nuri AKINCI*[1]

Abstract

Electromagnetic inverse scattering from high contrast scatterers is of special importance, especially in Microwave Imaging, wherein the recent technology aims to image high contrast scatterer. To this purpose, this paper presents an analysis of the performance of the recently proposed microwave imaging technique of the Near Field Orthogonality Sampling for the high contrast targets. For this purpose, the indicator of the Near Field Orthogonality Sampling Method, which is the reduced scattered field, is derived for an electrically homogeneous circular scatterer, which is centered around origin. The Near Field Orthogonality Sampling Method is classified in the qualitative microwave imaging techniques, which aim to retrieve only the shape and the position of the scatterers. Thus, the performance of the method can be assessed by comparing the energy of the indicator that falls in the exact target position with the energy that falls outside of the scatterer. Thus, the ratios of the indicator energy densities inside and outside of the target is defined as a quality metric. After, the quality metric and its expressions for limiting cases (i.e. where the electrical parameter of the the target is too large or too low) are derived in terms of the background's and target's electrical properties. Then, the introduced metric is computed and plotted for a popular application, which is microwave imaging of the breast. Obtained results show that the high contrasts between the target and the background does not have an important effect on the quality of the reconstructions of the Near Field Orthogonality Sampling Method.

Keywords: Near Field Orthogonality Sampling Method, Microwave Imaging, Bessel Functions, Hankel Functions

1. INTRODUCTION

Microwave imaging (MWI) is a recent arising technology that aims to sense the electrical properties of the targets by means of the measurements performed in microwave frequencies. It has a vast of applications in medical imaging [1]-[4], buried target imaging [5], [6], non-destructive testing [7]-[10]. Regardless of the application, one main problem of the microwave imaging is its non-linear nature, which comes from the multiple scattering effects. In [11], it is shown that the nonlinearity of the MWI increases with the increasing contrast of the target. Thus, imaging of high contrast scatterers is an important problem for any MWI technique.

Recently, a group of MWI techniques, which is called as qualitative MWI, starts to attract attention [12]–[14]. In particular, this class of MWI methods aims to retrieve only the shape of the target from scattered field measurements [13]. They are generally linear, non-iterative and cheaper in computational resource and time when compared with their quantitative analogues,

* Corresponding Author

Electronics and Communication Department, Istanbul Technical University[1]

which targets to retrieve the whole electrical parameter distribution on a pre-specified region [15], [16].

Near Field Orthogonality Sampling Method (NOSM) was proposed in a recent work of the author [17], [18]. Besides possessing all attractive features of qualitative methods, the NOSM can also operate with single view - multi static measurements as well as having the capability of handling with multi-frequency data. Such properties makes NOSM useful in real-world scenarios. In this context, this paper investigates the performance of the NOSM for high-contrast targets. For this purpose, the reduced scattered electric field for an electrically homogeneous circular cylinder is derived for two dimensional-transverse magnetic (2D-TM) scattering configuration. By using the derived reduced electrical field a quality metric is defined. Next, the expression of the introduced quantity is obtained in terms of the electrical properties of the cylinder- the background medium and the radius of the cylindrical target. The quality metric is evaluated for a popular real world example, which is MWI of the breast. Obtained results show that contrary to quantitative MWI methods, which deeply influenced by the high contrast between the target and the background [11], the NOSM is not significantly effected by the high electrical parameter difference between the scatterer and the host medium.

2. NEAR FIELD ORTHOGONALITY SAMPLING METHOD APPLIED TO A CIRCULAR TARGET

The Near Field Orthogonality Sampling Method (NOSM) was introduced in [17]. In this section, we confine our analysis to particular case, which is the scattering from a circular target centered around origin.

2.1.1. Scattering From a Circular Target

Consider that a non-magnetic circular target Ω, whose radius is R and whose relative electrical permittivity-conductivity is $\epsilon_r - \sigma$ is centered to origin. The target is hosted in a non-magnetic background medium, whose electrical properties are

$\epsilon_{r,b} - \sigma_b$. The target is illuminated with plane waves, whose incidence angle is ϕ and whose polarization is of two dimensional transverse magnetic (2D-TM) scattering scenario. For this particular problem, the incident field on the target, the scattered field outside Ω and the total field inside the circle have to be in the following forms to be able to satisfy the sourceless Helmholtz equation [15]:

$$u_i(r,\theta) = \exp\big(-ik_b r cos(\phi-\theta)\big),\ \mathbf{r} = (r,\theta) \in \mathbf{R^2}$$
$$u_s(r,\theta) = \sum_{n=-\infty}^{\infty} A_n H_n^{(1)}(k_b r)\exp(in\theta),\ \mathbf{r} \in \mathbf{R^2/\Omega}$$
$$u_t(r,\theta) = \sum_{n=-\infty}^{\infty} B_n J_n(k_t r)\exp(in\theta),\ \mathbf{r} \in \mathbf{\Omega} \quad (1)$$

Then, the by employing the Maxwell's equation and noting that all mediums are non-magnetic the

corresponding magnetic fields can be derived as in the below [15]:

$$h(r,\theta) = \frac{i}{\omega\mu_0}\frac{\partial u(r,\theta)}{\partial r}$$

$$h_i(r,\theta) = \frac{i}{\omega\mu_0}\frac{\partial \exp\big(-ik_b r cos(\phi-\theta)\big)}{\partial r}$$

$$h_i(r,\theta) = \frac{i}{\omega\mu_0}\frac{\partial \sum_{n=-\infty}^{\infty} i^{-n} J_n(k_b r)\exp\big(-in(\phi-\theta)\big)}{\partial r}$$

$$= \frac{ik_b}{\omega\mu_0}\sum_{n=-\infty}^{\infty} i^{-n} J_n'(k_b r)\exp\big(-in(\phi-\theta)\big), \mathbf{r} \in \mathbf{R^2}$$

$$h_s(r,\theta) = \frac{ik_b}{\omega\mu_0}\sum_{n=-\infty}^{\infty} A_n H_n^{(1)\prime}(k_b r)\exp(in\theta), \mathbf{r} \in \mathbf{R^2/\Omega}$$

$$h_t(r,\theta) = \frac{ik_t}{\omega\mu_0}\sum_{n=-\infty}^{\infty} B_n J_n'(k_t r)\exp(in\theta), \mathbf{r} \in \mathbf{\Omega} \quad (2)$$

In (1) and (2), u-h are the electric field-the tangential component of the magnetic field, respectively; the subscripts i, s and t stands for the incident, scattered and total fields, respectively; $k_b = \sqrt{\omega^2\mu_0\epsilon_{r,b}\epsilon_0 + i\omega\mu_0\sigma_b}$, k_t are the wavenumbers in the host medium, target, respectively; μ_0, ϵ_0 are the magnetic permeability and electrical permittivity of the vacuum, respectively; $\omega = 2\pi f$ is the angular frequency of excitation; f is the frequency of the illumination; $J_n(\cdot)$ is the n[th] order Bessel function; $H_n^{(1)}(\cdot)$ is the n[th] order Hankel function of first kind and $(\cdot)'$ stands for the derivative of the related function. To determine the unknown coefficients, the continuity of the electric and tangential component of the magnetic fields have to be satisfied at r = R, thus we have:

$$u_i(\mathbf{r}) + u_s(\mathbf{r}) = u_t(\mathbf{r});\quad r = R, 0 \le \theta < 2\pi$$

$$\sum_{n=-\infty}^{\infty} i^{-n} J_n(k_b R)\exp\big(-in(\phi-\theta)\big) + A_n H_n^{(1)}(k_b R)\exp(in\theta) = \sum_{n=-\infty}^{\infty} B_n J_n(k_t R)\exp(in\theta);$$

$$i^{-n} J_n(k_b R)\exp(-in\phi) + A_n H_n^{(1)}(k_b R) = B_n J_n(k_t R); \quad (3)$$

$$h_i(\mathbf{r}) + h_s(\mathbf{r}) = h_t(\mathbf{r}); \quad r = R, 0 \le \theta < 2\pi$$

$$\sum_{n=-\infty}^{\infty} i^{-n} J_n'(k_b R)\exp\big(-in(\phi-\theta)\big) + A_n H_n^{(1)\prime}(k_b R)\exp(in\theta) = \frac{k_t}{k_b}\sum_{n=-\infty}^{\infty} B_n J_n'(k_t R)\exp(in\theta);$$

$$i^{-n} J_n'(k_b R)\exp(-in\phi) + A_n H_n^{(1)\prime}(k_b R) = \frac{k_t}{k_b} B_n J_n'(k_t R); \quad (4)$$

Solving (3) and (4) for one can find:

$$\frac{A_n}{i^{-n}\exp(-in\phi)} = \frac{k_t J_n(k_b R) J_n'(k_t R) - k_b J_n'(k_b R) J_n(k_t R)}{k_b H_n^{(1)\prime}(k_b R) J_n(k_t R) - k_t H_n^{(1)}(k_b R) J_n'(k_t R)}; \quad (5)$$

2.1.2. The Reduced Scattered Electric Field for Circular Target

In [17], the reduced scattered field is defined as in the below:

$$u_s^r(\mathbf{r}) = \int_{r'\in\mathbb{R}^2} J_0(k_b|\mathbf{r}-\mathbf{r}'|)\chi(\mathbf{r}')u(\mathbf{r}')d\mathbf{r}'; \mathbf{r}\in\mathbb{R}^2 \quad (6)$$

where $\chi = \frac{k^2}{k_b^2} - 1$ is the object function. Assume that the scattered field on the circle, whose center is origin and whose radius is ρ, is known. Then, from [17], it can be inferred that the reduced scattered field for $|\mathbf{r}| < \rho$ may be calculated as:

$$u_s^r(\mathbf{r}) = \int_{r'\in\mathbb{R}^2} K(\mathbf{r},\mathbf{q}) u_s(\mathbf{q},\phi) d\mathbf{q};$$

$$|\mathbf{r}| < \rho, \mathbf{q} = (q,\alpha) \quad (7)$$

where the kernel of the operator is given as [17]:

$$K(\mathbf{r},\mathbf{q}) = -\frac{2i}{\pi\rho}\sum_{n=-\infty}^{\infty}\frac{J_n(k_b r)}{H_n^{(1)}(k_b\rho)}\exp\big(in(\theta-\alpha)\big); \; |\mathbf{r}| < \rho, \mathbf{q} = (q,\alpha) \quad (8)$$

Combining (1), (7) and (8), one can show that:

$$u_s^r(\mathbf{r}) = \int_{\alpha=0}^{2\pi} -\frac{2i}{\pi\rho}\sum_{m=-\infty}^{\infty}\frac{J_m(k_b r)}{H_m^{(1)}(k_b\rho)}\exp\big(im(\theta-\alpha)\big)\sum_{n=-\infty}^{\infty} A_n H_n^{(1)}(k_b q)\exp(in\alpha)\, q\, d\alpha;$$

$$= \frac{2i}{\pi\rho}\sum_{m=-\infty}^{\infty}\frac{J_m(k_b r)}{H_m^{(1)}(k_b\rho)}\sum_{n=-\infty}^{\infty} A_n H_n^{(1)}(k_b q)\, q$$

$$\int_{\alpha=0}^{2\pi}\exp(im(\theta-\alpha)+in\alpha)d\alpha$$

$$= \frac{2i}{\pi\rho}\sum_{m=-\infty}^{\infty}\frac{J_m(k_b r)}{H_m^{(1)}(k_b\rho)}\sum_{n=-\infty}^{\infty} A_n H_n^{(1)}(k_b q)\, q$$

$$2\pi\delta_{m-n}\exp(im\theta)$$

$$= -4i\sum_{n=-\infty}^{\infty} A_n J_n(k_b r)\exp(in\theta) \quad (9)$$

where $\delta_{(\cdot)}$ stands for the well-known discrete delta function.

2.1.3. The Quality Metric

Our interest is understanding the performance of the NOSM with changing contrast between the target and the host medium. The NOSM states that the norm of the u_s^r of (9) is relatively larger at those points, which fall into a target; and conversely, the norm of u_s^r of (9) is relatively lower at those points, which falls into the background. For the particular case that is investigated above, the target is a circle with radius R. Assume that the target is known to be encapsulated in a circular domain D, whose radius is R_D. The indicator function of the NOSM becomes:

$$I(\mathbf{r}) = |u_s^r(\mathbf{r})|^2; \quad \mathbf{r}\in D \quad (10)$$

Thus, a quality metric can be defined as in the below:

$$Q = \frac{\int_{r\in\Omega}\frac{I(r)}{S_\Omega}dr}{\int_{r\in\mathrm{D}}\frac{I(r)}{S_\mathrm{D}}dr} \quad (11)$$

where $S_\Omega = \pi R^2$ and $S_D = \pi R_D^2$ are the areas of target and the investigation domain, respectively. Note that, in ideal case $Q = \frac{S_D}{S_\Omega}$, since $I(\mathbf{r}) = 0$ for $\mathbf{r}\in D-\Omega$. Here, the following closed form expression can be obtained for the quality metric:

$$Q = \frac{\int_{r\in\Omega}\frac{\left|-4i\sum_{n=-\infty}^{\infty} A_n J_n(k_b r)\exp(in\theta)\right|^2}{S_\Omega}dr}{\int_{r\in\mathrm{D}}\frac{\left|-4i\sum_{n=-\infty}^{\infty} A_n J_n(k_b r)\exp(in\theta)\right|^2}{S_\mathrm{D}}dr}$$

$$= \frac{\sum_{n=-\infty}^{\infty}|A_n|^2\int_{r=0}^{R} J_n(k_b r)^2 r dr}{\sum_{n=-\infty}^{\infty}|A_n|^2\int_{r=0}^{R_D} J_n(k_b r)^2 r dr}$$

$$= \frac{\sum_{n=-\infty}^{\infty}|A_n|^2 R^2(J_n^2 - J_{n-1}J_{n+1}(k_b R))}{\sum_{n=-\infty}^{\infty}|A_n|^2 R_D^2(J_n^2 - J_{n-1}J_{n+1}(k_b R_D))} \quad (12)$$

Thus, as seen from (12), the quality metric is a function of the electrical lengths of $k_b R$, $k_t R$ and $k_b R_D$.

2.1.4. Analysis of Quality Metric for High Contrast Case

In the high contrast situation, the difference between the background and target wavenumber gets larger. In most of the applications, electrical parameters of the background is both adjustable and also confined to a limited range, while the electrical parameters of the

targets can vary in wider area. Thus, we may analyze the quality metric derived in (12) for two different situation: (i) $|k_tR| > |k_bR|$, i.e. as $|k_tR| \to \infty$; (ii) $|k_tR| < |k_bR|$, i.e. as $|k_tR| \to 0$.

Let us first investigate the case in (i), i.e. $|k_tR| \to \infty$. For large arguments the Bessel function has the following asymptotic form [15]:

$$J_n(k_tR) \sim \sqrt{\frac{2}{\pi k_tR}}\cos\left(k_tR - \frac{n\pi}{2} - \frac{\pi}{4}\right) \tag{13}$$

Then the asymptotic properties of the derivative can be derived as:

$$J_n'(k_tR) = \frac{J_{n-1}(k_tR) - J_{n+1}(k_tR)}{2}$$

$$\sim \sqrt{\frac{2}{\pi k_tR}}\,\frac{\cos\left(k_tR - \frac{(n-1)\pi}{2} - \frac{\pi}{4}\right) - \cos\left(k_tR - \frac{(n+1)\pi}{2} - \frac{\pi}{4}\right)}{2}$$

$$\sim \sqrt{\frac{2}{\pi k_tR}}\,\frac{-2\sin(k_tR - \frac{n\pi}{2} - \frac{\pi}{4})\sin(\frac{\pi}{2})}{2}$$

$$\sim -\sqrt{\frac{2}{\pi k_tR}}\,\sin(k_tR - \frac{n\pi}{2} - \frac{\pi}{4}) \tag{14}$$

Employing the asymptotic forms of the Bessel function and its derivative the followings can be obtained:

$$\frac{J_n(k_tR)}{k_tJ_n'(k_tR)} \sim \frac{\sqrt{\frac{2}{\pi k_tR}}\cos\left(k_tR - \frac{n\pi}{2} - \frac{\pi}{4}\right)}{-k_t\sqrt{\frac{2}{\pi k_tR}}\sin(k_tR - \frac{n\pi}{2} - \frac{\pi}{4})}$$

$$\sim -\frac{1}{k_t}\cot\left(k_tR - \frac{n\pi}{2} - \frac{\pi}{4}\right) \tag{15}$$

Here $k_tR = p\exp(i\theta)$ where $p \to \infty$ and $0 \le \theta < 2\pi$. Thus, letting $\beta = k_tR - \frac{n\pi}{2} - \frac{\pi}{4} = \alpha + i\gamma$, it is easy see that $\alpha \ge -\frac{n\pi}{2} - \frac{\pi}{4}$ and $\gamma \ge 0$. Therefore, the followings are true:

$$\cot(\beta) = \frac{\cos(\beta)}{\sin(\beta)} = i\,\frac{\exp(i\beta)+\exp(-i\beta)}{\exp(i\beta)-\exp(-i\ )}$$

$$= i\,\frac{\exp(i\alpha)\exp(-\gamma)+\mathrm{e}\quad(-i\ )\exp(\gamma)}{\exp(i\alpha)\exp(-\gamma)-\exp(-i\alpha)\exp(\gamma)}$$

$$\sim i\,\frac{\exp(-i\alpha)\exp(\gamma)}{-\exp(-i\alpha)\exp(\gamma)} \sim -i \tag{16}$$

Thus, using (5), we may obtain the asymptotic expression for $|A_n|$ of (12):

$$|A_n| = \left|\frac{J_n(k_bR) - k_bJ_n'(k_bR)\frac{J_n(k_tR)}{k_tJ_n'(k_tR)}}{k_bH_n^{(1)'}(k_bR)\frac{J_n(k_tR)}{k_tJ_n'(k_tR)} - H_n^{(1)}(k_bR)}\right|$$

$$\sim \left|\frac{J_n(k_bR) - J_n'(k_bR)\frac{i}{k_t}}{k_bH_n^{(1)'}(k_bR)\frac{i}{k_t} - H_n^{(1)}(k_bR)}\right| \sim \left|\frac{J_n(k_bR)}{H_n^{(1)}(k_bR)}\right| \tag{17}$$

Thus, for large contrast of the target, the quality factor becomes only a function of wavenumber of the background.

Now, let us investigate the case in (ii), i.e. $|k_tR| \to 0$. For small arguments, the Bessel function has the following asymptotic form [15]:

$$J_n(k_tR) \sim \frac{\left(\frac{k_tR}{2}\right)^n}{n!} \tag{18}$$

Then, the derivative of the Bessel function has the following asymptotic form:

$$J_n'(k_tR) = \frac{J_{n-1}(k_tR) - J_{n+1}(k_tR)}{2}$$

$$\sim \frac{\frac{\left(\frac{k_tR}{2}\right)^{n-1}}{(n-1)!} - \frac{\left(\frac{k_tR}{2}\right)^{n+1}}{(n+1)!}}{2} \sim \frac{\left(\frac{k_tR}{2}\right)^{n-1}}{(n-1)!}\,\frac{1 - \frac{\left(\frac{k_tR}{2}\right)^2}{n(n+1)}}{2}$$

$$\sim \frac{\left(\frac{k_tR}{2}\right)^{n-1}}{2(n-1)!} \tag{19}$$

Therefore, the following expression can be derived:

$$\frac{J_n(k_tR)}{k_tJ_n'(k_tR)} \sim \frac{\frac{\left(\frac{k_tR}{2}\right)^n}{n!}}{k_t\frac{\left(\frac{k_tR}{2}\right)^{n-1}}{2(n-1)!}} \sim \frac{2}{k_t}\frac{k_tR}{2n} \sim \frac{R}{n} \tag{20}$$

Thus, the asymptotic form of $|A_n|$ of (12) for small contrast of the target becomes:

$$|A_n| = \left|\frac{J_n(k_bR) - k_bJ_n'(k_bR)\frac{J_n(k_tR)}{k_tJ_n'(k_tR)}}{k_bH_n^{(1)'}(k_bR)\frac{J_n(k_tR)}{k_tJ_n'(k_tR)} - H_n^{(1)}(k_bR)}\right|$$

$$\sim \left|\frac{J_n(k_bR) - \frac{k_bJ_n'(k_bR)R}{n}}{\frac{k_bH_n^{(1)'}(k_bR)R}{n} - H_n^{(1)}(k_bR)}\right|$$

$$\sim \left|\frac{J_n(k_bR) - \frac{k_bR}{n}J_n'(k_bR)}{\frac{k_bR}{n}H_n^{(1)'}(k_bR) - H_n^{(1)}(k_bR)}\right| \tag{21}$$

3. ANALYSIS OF QUALITY METRIC

In this section, the performance of the NOSM is assessed by analyzing the quality metric for a popular real-world problem, which is imaging of breast with microwaves [2], [4], [20]–[25]. There are many different algorithms applied for microwave imaging of breast: quantitative inversion methods [20]–[23],

surface impedance based technique [2], radar based approaches [24], [25]. Regardless of the utilized approach, one common problem is the higher contrast of the fibroglandular tissues inside the breast [11]. The higher contrast limits the performance of microwave imaging from two aspects: (i) A coupling medium is required to enhance the penetration of the waves inside the breast [2], [21]. (ii) The non-linearity of the inverse scattering mechanism increases if the difference between the mean contrast of the breast and the background gets larger [11].

Here, we note that the relative electrical permittivity of the tissues inside the breast is between 1-80. Thus, the relative electrical permittivity of the background and the target are limited in this interval, i.e. $1 \leq \epsilon_{r,b}, \epsilon_{r,t} \leq 80$. Firstly, it is assumed that both the background and the target are lossless, i.e. $\sigma_b = \sigma_t = 0\frac{S}{m}$. The radius the breast is taken as $R = 5\ cm$ and the investigation domain is selected such that $R_D = 15\ cm$. The quality metric is calculated and normalized with S_D/S_Ω for all $\epsilon_{r,b} - \epsilon_{r,t}$ couple by sweeping 1-80 interval with a constant step size of 0.1. The results for 0.5 GHz, 1 GHz, 1.5 GHz and 2 GHz are given in Figure 1(a) - Figure 1(d). As seen from these results, the quality metric is changing between 0.1-0.45, while mostly $\frac{Q}{S_D/S_\Omega}$ is around 0.3. Thus, as can be seen from these results, the quality of the obtained images are not influenced from the high contrast between the target and the background, which is an advantage of the NOSM over conventional non-linear optimization methods.

As second test, the quality metric for a conductive breast is evaluated. Here all parameters of the setup is the same of the previous case except the conductivity of breast, which is taken as 1.5 S/m. Note that such a conductivity corresponds to a high value with respect to the conductivities of the realistic breast models given in [19]. The results for this case is given in Figure 2(a) - Figure 2(d) for 0.5 GHz, 1 GHz, 1.5 GHz and 2 GHz, respectively. As can be observed from these results the quality remains between 0.2 - 0.3. Thus, similar to the lossless case, the quality of the obtained reconstructions does not exhibit a significant variation for high contrasts between the target and the background.

Lastly, the extreme cases, where the contrast of the scatterer is very large (i.e. $|k_t R| \to \infty$) - very low (i.e. $|k_t R| \to 0$) are investigated in Figure 3-Figure 4, respectively. For that purpose the quality factors in limiting cases, are plotted in Figure 3-Figure 4 for $|k_t R| \to \infty - |k_t R| \to 0$ by setting $|A_n|$ of (12) to the expressions, which are derived in (17)-(21). Here, by observing through Figure 3(a)-Figure 3(d), it can be seen that the quality factors are limited in 0.2-0.35 range as $|k_t R| \to \infty$. Similar to $|k_t R| \to \infty$ case, by observing the results for $|k_t R| \to 0$, which are given in Figure 4(a)-Figure 4(d), the quality factor is seen to be confined almost in the same range. As in the previous situations, these results imply that in contrast to quantitative approaches, which profoundly influenced by the high contrast between the target and the background [11], the quality of the reconstructions obtained by NOSM does not significantly vary with the increasing electrical parameter between the target and the background medium.

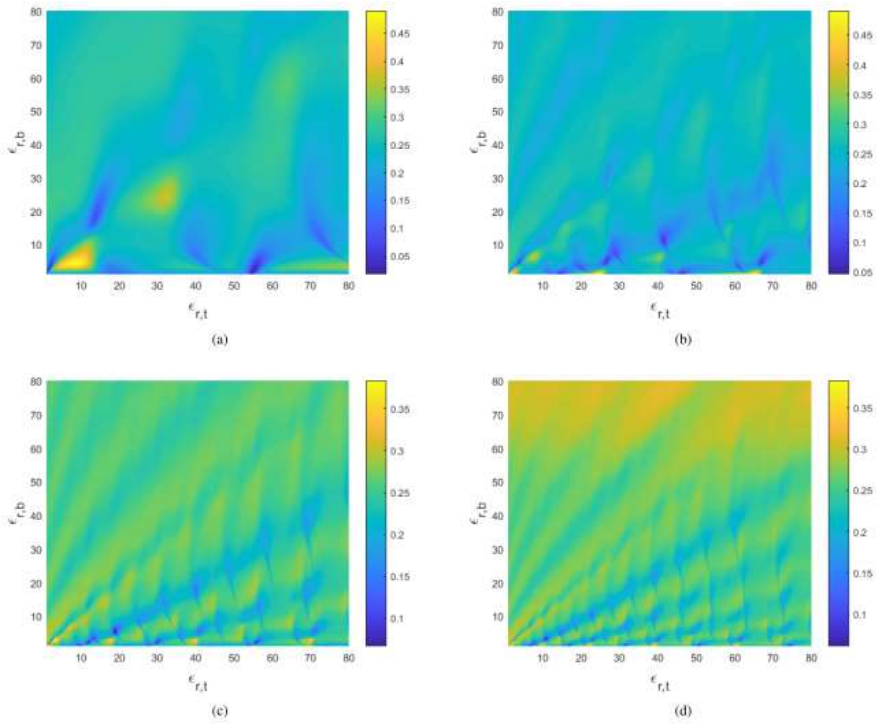

Figure 1. Quality metric for microwave breast imaging with NOSM. The relative permittivities of the background and the breast tissues are swept between 1-80 with a constant step size of 0.1. For this result, the breast and background are assumed to be lossless

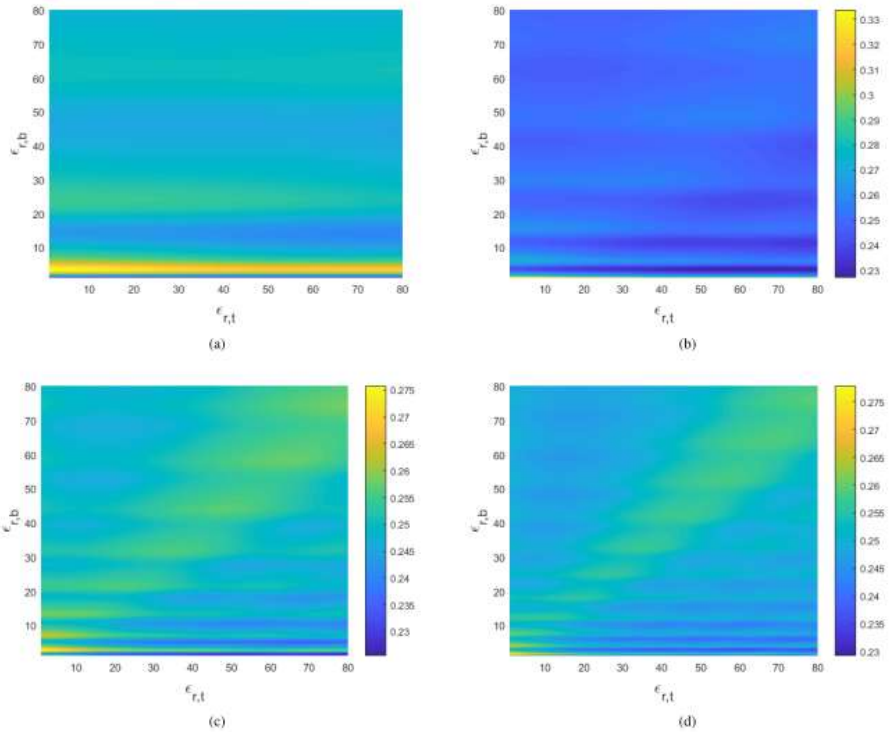

Figure 2. Quality metric for microwave breast imaging with NOSM. The relative permittivities of the background and the breast tissues are swept between 1-80 with a constant step size of 0.1. For this result, the background is assumed to be lossless but the breast is assumed to have a conductivity of $\sigma_t = 1.5$ S/m. Note that such a conductivity corresponds a large value that can be observed from the breast models in [19].

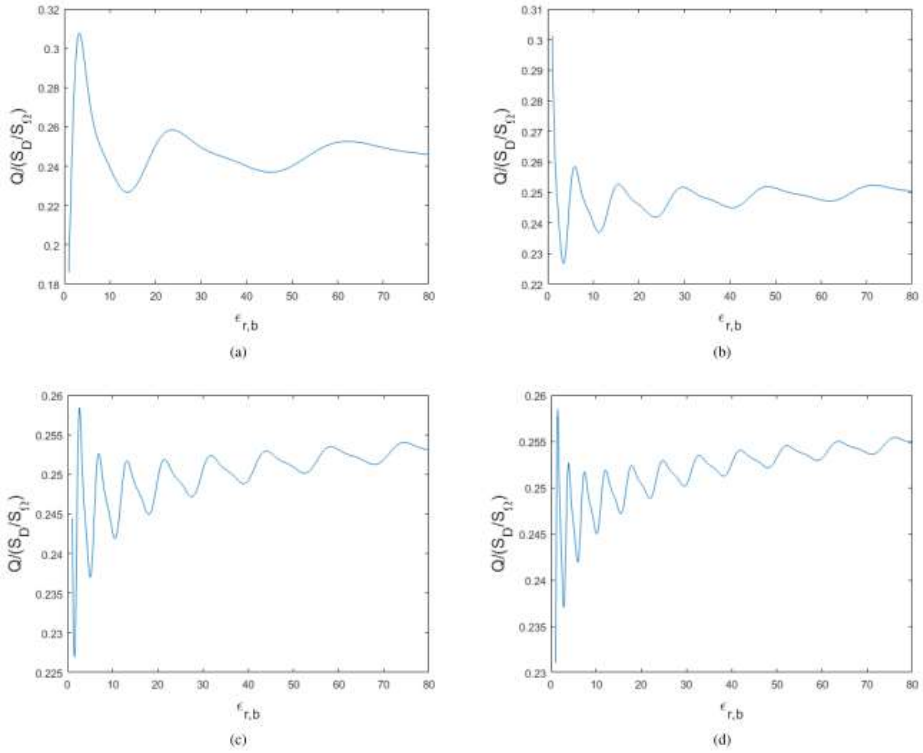

Figure 3. Quality metric for microwave breast imaging with NOSM when the contrast of target is very large (i.e. as $|k_t R| \to \infty$). Here the relative permittivity of the background is swept between 1-80 with a constant step size of 0.1. For this result, the background is assumed to be lossless

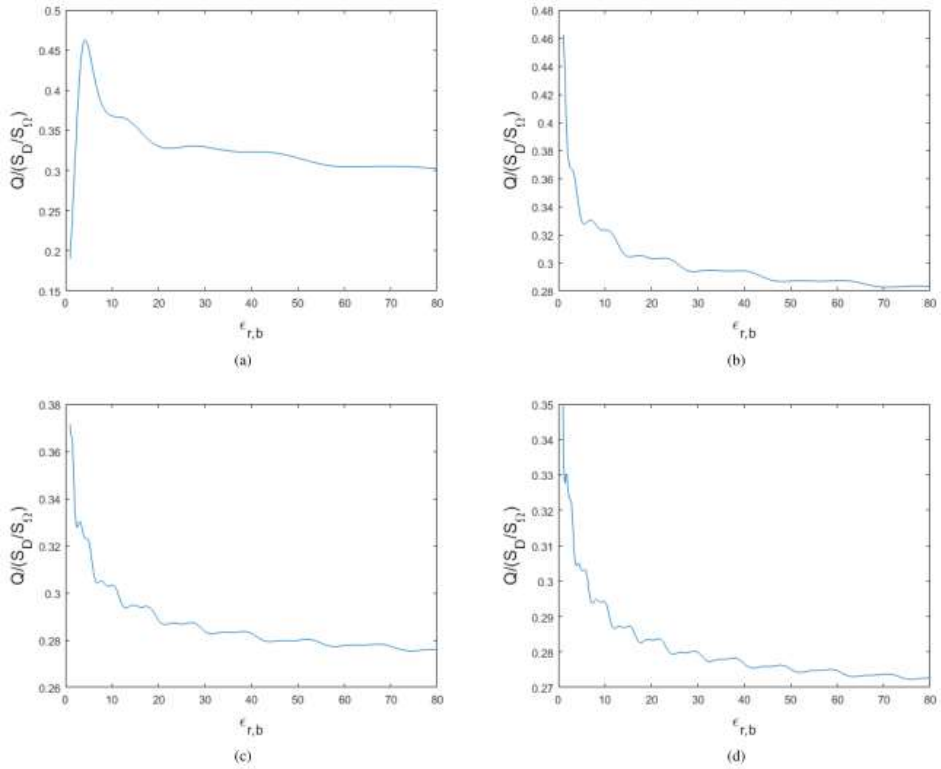

Figure 4. Quality metric for microwave breast imaging with NOSM when the contrast of target is very low (i.e.as $|k_t R| \to 0$). Here the relative permittivity of the background is swept between 1-80 with a constant step size of 0.1. For this result, the background is assumed to be lossless

4. CONCLUSION

In this paper, the quality of the reconstructions of a recently proposed qualitative microwave imaging (MWI) approach, which is named as Near Field Orthogonality Sampling Method (NOSM), is investigated. For this aim, a simplistic example, which is scattering from a circular cylinder, has been employed. The scattered fields from the cylinder has been derived first. Then, the indicator function of the NOSM, which is the reduced scattered field, has been derived for the considered special case. After deriving the expression for reduced scattered field, a quality metric has been defined and the expression of the introduced metric is given in terms of the electrical lengths of the scatterer. Here, for better understanding the effect of the high contrast situation, the expressions of the quality metric for $|k_t R| \to \infty$ and $|k_t R| \to 0$ have been derived. The derived quality metrics are numerically analyzed for MWI of the breast case. Obtained results show that the quality of the NOSM has been confined into a narrow interval for all contrasts, which is a good behavior compared to the quantitative MWI approaches, whose non-linearity is inherently linked to high contrast between the target and the host medium.

REFERENCES

[1] D. Ireland, K. Bialkowski, and A. Abbosh, "Microwave imaging for brain stroke detection using born iterative method," IET Microwaves, Antennas & Propagation, vol. 7, no. 11, pp. 909–915, 2013.

[2] O. Güren, M. Çayören, L. T. Ergene, and I. Akduman, "Surface impedance based microwave imaging method for breast cancer screening: contrast-enhanced scenario," Physics in Medicine & Biology, vol. 59, no. 19, p. 5725, 2014.

[3] E. Balidemaj, C. A. van den Berg, J. Trinks, A. L. van Lier, A. J. Nederveen, L. J. Stalpers, H. Crezee, and R. F. Remis, "Csi-ept: A contrast source inversion approach for improved mri-based electric properties tomography," IEEE transactions on medical imaging, vol. 34, no. 9, pp. 1788–1796, 2015.

[4] Z. Miao and P. Kosmas, "Multiple-frequency dbim-twist algorithm for microwave breast imaging," IEEE Transactions on Antennas and Propagation, 2017.

[5] Ö. Özdemir and H. Haddar, "Preprocessing the reciprocity gap sampling method in buried-object imaging experiments," IEEE Geoscience and Remote Sensing Letters, vol. 7, no. 4, pp. 756–760, 2010.

[6] M. Bevacqua, L. Crocco, L. D. Donato, T. Isernia, and R. Palmeri, "Exploiting sparsity and field conditioning in subsurface microwave imaging of nonweak buried targets," Radio Science, vol. 51, no. 4, pp. 301–310, 2016.

[7] E. Bilgin and A. Yapar, "Electromagnetic scattering by radially inhomogeneous dielectric spheres," IEEE Transactions on Antennas and Propagation, vol. 63, no. 6, pp. 2677–2685, 2015.

[8] F. Boero, A. Fedeli, M. Lanini, M. Maffongelli, R. Monleone, M. Pastorino, A. Randazzo, A. Salvad`e, and A. Sansalone, "Microwave tomography for the inspection of wood materials: Imaging system and experimental results," IEEE Transactions on Microwave Theory and Techniques, 2018.

[9] M. N. Akıncı, T. Caglayan, S. Ozgur, U. Alkası, H. Ahmadzay, M. Abbak, M. C¸ ay¨oren, and ˙I. Akduman, "Qualitative microwave imaging with scattering parameters measurements," IEEE Transactions on Microwave Theory and Techniques, vol. 63, no. 9, pp. 2730–2740, 2015.

[10] G. Govind and M. Akhtar, "Microwave nondestructive imaging of buried objects using improved scattered-field calibration technique," Radio Science, vol. 53, no. 1, pp. 2–14, 2018.

[11] O. M. Bucci, N. Cardace, L. Crocco, and T. Isernia, "Degree of nonlinearity and a new solution procedure in scalar two-dimensional inverse scattering problems," JOSA A, vol. 18, no. 8, pp. 1832–1843, 2001.

[12] A. Kirsch, "The music-algorithm and the factorization method in inverse scattering theory for inhomogeneous media," Inverse problems, vol. 18, no. 4, p. 1025, 2002.

[13] R. Potthast, "A survey on sampling and probe methods for inverse problems," Inverse Problems, vol. 22, no. 2, p. R1, 2006.

[14] F. Cakoni, D. Colton, and P. Monk, The Linear Sampling Method in Inverse Electromagnetic Scattering. SIAM-Society for Industrial and Applied Mathematics, 2010.

[15] W. Chew and Y. Wang, "Reconstruction of two-dimensional permittivity distribution using the

distorted born iterative method," Medical Imaging, IEEE Transactions on, vol. 9, no. 2, pp. 218–225, 1990.

[16] A. Abubakar, P. M. Van den Berg, and J. J. Mallorqui, "Imaging of biomedical data using a multiplicative regularized contrast source inver-

sion method," IEEE Transactions on Microwave Theory and Techniques, vol. 50, no. 7, pp. 1761–1771, 2002.

[17] M. N. Akıncı, M. Cayoren, and I. Akduman, "Near-field orthogonality sampling method for microwave imaging: Theory and experimental verification," IEEE Transactions on Microwave Theory and Techniques, vol. 64, no. 8, pp. 2489–2501, 2016.

[18] M. N. Akinci, "Improving near field orthogonality sampling method for qualitative microwave imaging," IEEE Transactions on Antennas and Propagation, 2018.

[19] The uwcem numerical breast phantom repository, university of wisconsin. [Online]. Available: http://uwcem.ece.wisc.edul home.htm.

[20] G. Bellizzi, O. M. Bucci, and I. Catapano, "Microwave cancer imaging exploiting magnetic nanoparticles as contrast agent," Biomedical Engineering, IEEE Transactions on, vol. 58, no. 9, pp. 2528–2536, 2011.

[21] M. T. Bevacqua and R. Scapaticci, "A compressive sensing approach for 3d breast cancer microwave imaging with magnetic nanoparticles as contrast agent," IEEE transactions on medical imaging, vol. 35, no. 2, pp. 665–673, 2016.

[22] J. D. Shea, P. Kosmas, S. C. Hagness, and B. D. Van Veen, "Contrast-enhanced microwave breast imaging," in Antenna Technology and Applied Electromagnetics and the Canadian Radio Science Meeting, 2009. ANTEM/URSI 2009. 13th International Symposium on. IEEE, 2009, pp. 1–4.

[23] J. D. Shea, P. Kosmas, B. D. Van Veen, and S. C. Hagness, "Contrast-enhanced microwave imaging of breast tumors: a computational study using 3D realistic numerical phantoms," Inverse Problems, vol. 26, no. 7, p. 074009, Jul 2010.

[24] D. Smith, O. Yurduseven, B. Livingstone, and V. Schejbal, "Microwave imaging using indirect holographic techniques," IEEE Antennas and Propagation Magazine, vol. 56, no. 1, pp. 104–117, 2014.

[25] E. J. Bond, X. Li, S. C. Hagness, and B. D. Van Veen, "Microwave imaging via space-time beamforming for early detection of breast cancer," IEEE Transactions on Antennas and Propagation, vol. 51, no. 8, pp. 1690–1705, 2003.